https://doi.org/10.17221/120/2026-RAE

Integrating Sentinel-1 SAR and Sentinel-3 SLSTR data with a random forest algorithm for evapotranspiration estimation in Malaysian durian orchards

Abhikrishnan Gopakumar[1], *Siva Kumar Balasundram*[1]*, *Christopher Boon Sung Teh*[2], *Wan Fazilah Fazlil Ilahi*[1]

[1]*Department of Agricultural Technology, Faculty of Agriculture, Universiti Putra Malaysia, Serdang, Selangor, Malaysia*
[2]*Department of Land Management, Faculty of Agriculture, Universiti Putra Malaysia, Serdang, Selangor, Malaysia*

**Corresponding author: siva@upm.edu.my*

Citation: Gopakumar A., Balasundram S.K., Teh C.B.S., Ilahi W.F.F. (2026): Integrating Sentinel-1 SAR and Sentinel-3 SLSTR data with a random forest algorithm for evapotranspiration estimation in Malaysian durian orchards. Res. Agr. Eng., XX: 00–00.

Abstract: A remote sensing-based methodology is adopted to estimate evapotranspiration in Malaysian durian orchards by integrating Sentinel-1 and Sentinel-3 datasets. Reference evapotranspiration data were obtained from the MODIS satellite and the weather station in the study area. The collected data were incorporated into a random forest machine learning algorithm to estimate evapotranspiration. Two models were developed using the reference data collected from the satellite and the weather station, and both models were statistically significant. The model with MODIS reference data achieved an *r* value of 0.971 and a root mean square error (RMSE) of 0.191 mm for calibration, and 0.913 and 0.885 mm for validation, respectively. The validation is performed using a temporally independent dataset drawn from three months before and after the primary sampling period. Similarly, the model with weather station reference data achieved an *r* value of 0.990 and an RMSE of 0.710 mm for calibration, and 0.998 and 0.215 mm for validation, respectively. This study demonstrates the utility of high-resolution satellite data combined with artificial intelligence in estimating evapotranspiration with reasonable accuracy at a low cost.

Keywords: irrigation management; machine learning; precision agriculture; remote sensing; tropical fruit

Evapotranspiration (ET) represents the combined release of water through evaporation from the land and water surfaces and the transpiration from plant leaves, which is a critical component of the hydrological cycle (Shang et al. 2024). Various applications like water resource management, agricultural planning and climate change studies require accurately estimated ET. The introduction of remote sensing and artificial intelligence (AI) has contributed a lot to monitoring and estimating ET over large areas with greater accuracy and resolution. ET is inevitable in irrigation scheduling, crop water requirements and overall water use efficiency in agricultural systems (Guo et al.

Supported by Top Fruits Sdn. Bhd. Vote No. 6300504. This research is part of a joint project with UPM and Top Fruits Sdn. Bhd. Entitled Assessment of Nutrient Use Efficiency and Water Use Efficiency in Selected Tropical Fruit Crops using Data-driven Approaches.

© The authors. This work is licensed under a Creative Commons Attribution 4.0 International (CC NC 4.0).

https://doi.org/10.17221/120/2026-RAE

2025). Precise ET estimation becomes more critical for ensuring sustainable water management, since the global population is rapidly growing and climate change impacts become more pronounced (Kebede et al. 2025).

Traditional ET estimation techniques, like lysimeter measurements and eddy covariance techniques, provide accurate point-scale values but are limited in their large-scale coverage and are often costly to implement on larger areas (Rahman et al. 2025). The Sentinel program of the European Space Agency (ESA) has significant attention among other satellite missions due to its high resolution and free availability of products. The introduction of synthetic aperture radar (SAR) and sea and land surface temperature radiometer (SLSTR) provides valuable information and makes the ET estimation accurate (Guo et al. 2024). SAR data were combined with SLSTR thermal data in this study primarily to overcome the persistent cloud cover characteristic of the humid tropical climate of Malaysia, since SAR signals penetrate cloud cover and are largely unaffected by atmospheric conditions, whereas optical and thermal sensors such as SLSTR are not; this combination therefore ensures a more temporally consistent data record for ET modelling. These sensors provide data on surface properties, vegetation quality and thermal characteristics, which are crucial components for developing ET models (Das et al. 2023). In recent years, there have been significant advancements made by AI, specifically machine learning, in parallel with the developments in remote sensing. Various machine learning algorithms like random forest (RF) (Hailegnaw et al. 2024), support vector machine (SVM) (Jia et al. 2022) and gradient boosting machine (GBM) (Naghdyzadegan Jahromi et al. 2023) have shown exceptional capabilities in handling non-linear, complex relationships between input variables and target outcomes (Chipula et al. 2025). This makes them a good fit for ET estimation, where various biophysical, climatic and environmental parameters interact intrinsically to influence ET. The integration of remotely sensed data with AI techniques develops a powerful method to improve the accuracy of ET estimation (Zolfaghari et al. 2025). By leveraging the strengths of both domains, researchers can develop more robust and adaptable models that can account for the diverse conditions encountered across different landscapes and climatic regions.

Various studies have effectively estimated and predicted the spatiotemporal variability of ET in different global scales, adopting several methodologies, including the surface energy balance algorithm (SEBAL) (Silva et al. 2025), two source model (TSM) (Bu et al. 2024), surface energy balance system (SEBS) (Bai et al. 2024), atmosphere land exchange inverse model (ALEXI) (Fuentes et al. 2024), Surface energy balance index (SEBI) (Woldemariam et al. 2025) and the ETA mapping algorithm (ETMA)(Aguirre-García et al. 2021). In order to minimise the uncertainties in the ET estimation, Knipper et al. (2024) proposed a more advanced methodology using remote sensing and machine learning techniques. Recently, various studies have focused on quantifying and estimating ET. The application of Sentinel-2 and Sentinel-3 spectral data provides critical and appropriate information for estimating ET, even with spatial resolutions ranging from 10 m to 1 km. Similarly, the project Sen ET (https://www.esa-sen4et.org) has demonstrated that Sentinel-2 high-resolution (10 to 60 m) multispectral data, combined with Sentinel-3 moderate-resolution (1 km) thermal data, yielded a reliable and accurate ET estimate. Another study by Allam et al. (2021) showed the importance of remote sensing in drought monitoring and estimated ET using multispectral data. Although remote sensing data is widely used in agricultural research, there have been very few studies in Malaysia on integrating machine learning with remote sensing data, particularly for estimating ET. In this regard, the real-time monitoring and balance of water resource usage require the examination of various parameters, specifically vertical-vertical backscatter intensity (VV), vertical-horizontal backscatter intensity (VH), difference of VV and VH (VV-VH), and ratio of VV and VH (VV/VH), which are seldom used in previous studies (Fan et al. 2025). The introduction of these parameters derived from Sentinel 3 data, such as the normalised difference vegetation index (NDVI) and land surface temperature (LST), provides highly reliable spectral information on ET (Musyimi et al. 2022). This method conflicts with existing methods such as pan evaporation, lysimetric, and eddy covariance, which require extensive field data (Kebede et al. 2025). The limitations of meteorological data necessitate the use of alternative methods to estimate ET. The objectives of this study were to (*i*) integrate Sentinel-1 SAR and Sentinel-3 SLSTR data with

https://doi.org/10.17221/120/2026-RAE

an RF algorithm to estimate evapotranspiration in a Malaysian durian orchard, and (*ii*) compare the performance of the RF model when calibrated using satellite-derived ET data against calibration using field-measured ET data.

MATERIAL AND METHODS

Study area. The study area was a 13-hectare commercial durian farm located in the district of Batu Pahat, Johor state, in Malaysia (1°41'N and 2°3'N, 102°42'E and 103°1'E) (Figure 1). The study region features a tropical humid climate with an annual average temperature of 27 °C throughout the year and yearly rainfall ranging from 2 000 to 2 500 mm. Batu Pahat district experiences consistent rainfall throughout the year, with the highest rainfall during the northeast monsoon from November to March. Mostly, the terrain is flat, with elevations varying from sea level to approximately 50 m inland. The district features extensive river systems, mainly the Batu Pahat River, which is the prominent one for irrigation and transportation. In coastal regions, the soil consists mainly of heavy clay and alluvial deposits, transitioning to fertile, loamy soils inland, enhancing agricultural suitability. Batu Pahat is renowned for its agricultural productivity, including various crops such as oil palm, rubber, coconut, and tropical fruits, including durian, rambutan, and jackfruit.

Data collection and pre-processing. The Sentinel-1 SAR ground range detected (GRD) and Sentinel-3 SLSTR Level 2 data were acquired biweekly for 2 years from January 2024 to December 2025 from the ESA Copernicus Dataspace Ecosystem (https://dataspace.copernicus.eu). The ET data from MODIS (MOD16A2), with a 500 m spatial resolution for the specified period, were acquired from the NASA Earthdata website (https://ladsweb.modaps.eosdis.nasa.gov/search/order/1/MOD16A2--61). ESA Sentinel-3 is a low Earth orbit mission part of the Copernicus programme, using the SLSTR dual-scan temperature radiometer. It has a wide range of applications, with a particular focus on sea surface temperature (SST) and terrestrial monitoring and evaluation (Guzinski

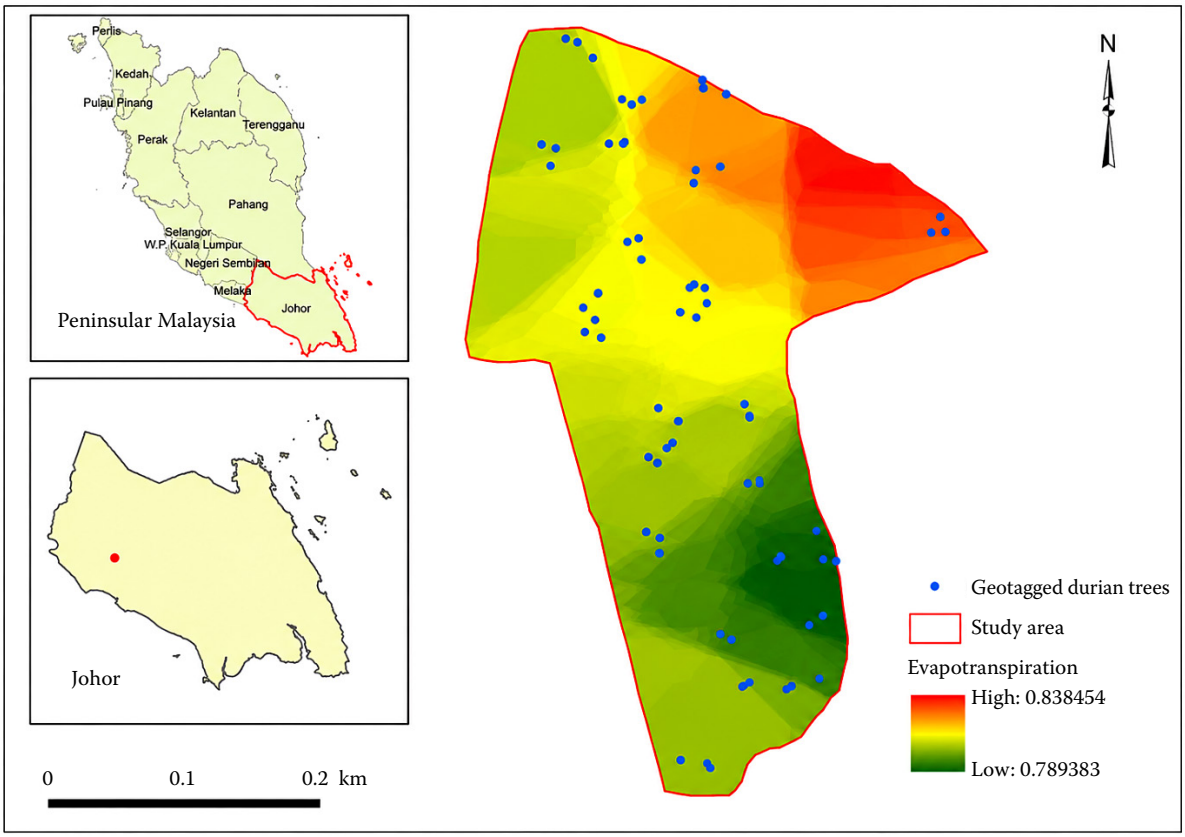


Figure 1. The study area map with the geo-tagged sampling trees

https://doi.org/10.17221/120/2026-RAE

Table 1. The list of remotely sensed variables and their descriptions

Variable	Description
NDVI	normalised difference vegetation index
LST	land surface temperature (°C)
FVC	fractional vegetation cover
TCWV	total column water vapour (kg/m^2)
VV	vertical-vertical backscatter intensity in decibels (dB)
VH	vertical-horizontal backscatter intensity in decibels (dB)
VH-VV	difference between VH and VV (dB)
VH/VV	ratio of VH and VV (dB)
RVI	radar vegetation index (dB), {4 × VH/(VH + VV)}

and Nieto 2019). The Sentinel-3 mission provides data with moderate spatial resolution and high temporal resolution, enabling precise global and regional SST and land surface temperature (LST) estimates (Hu et al. 2019). The data are influenced by factors such as moisture content, vegetation cover, and surface heterogeneity, making interpretation difficult. SAR captures high-resolution radar backscatter from terrain, observing both geophysical and biological elements (Fan et al. 2025). The surface features include physical attributes like geometric shape, surface roughness and digital elevation models.

The preprocessing of Sentinel-1 GRD radar data includes removal of thermal and border noise, co-registration, insertion of orbit file, radiometric calibration, and geometric correction with Range-Doppler terrain correction. Finally, speckle filtering was performed using a three-by-three Lee filter (Shamsaie and Ghaderi 2025). Using the band math tool in the Sentinel application platform (SNAP) software version 13, the difference of VH and VV (VH-VV), the ratio of VH and VV (VH/VV), and the radar vegetation index (RVI) (Santos et al. 2025) were calculated and then all these parameters were converted to the decibel scale. This conversion compresses the multi-order radar signal intensities into a manageable, normal distribution that improves sensitivity to changes in surface soil moisture and vegetation canopy structure. The level 2 SLSTR Sentinel-3 datasets were co-registered, geometrically corrected, and resampled to a spatial resolution of 10 m. Vegetative parameters, including NDVI, LST, FVC, and TCWV, were retrieved from the processed Sentinel-3 data. The LST data is originally in Kelvin, it was converted into degree Celsius (°C) using the ArcMap software version 10.8. The remotely sensed Sentinel variables are listed in Table 1. The MODIS ET raster data were clipped to the study area after resampling to 10 m and applying a scale

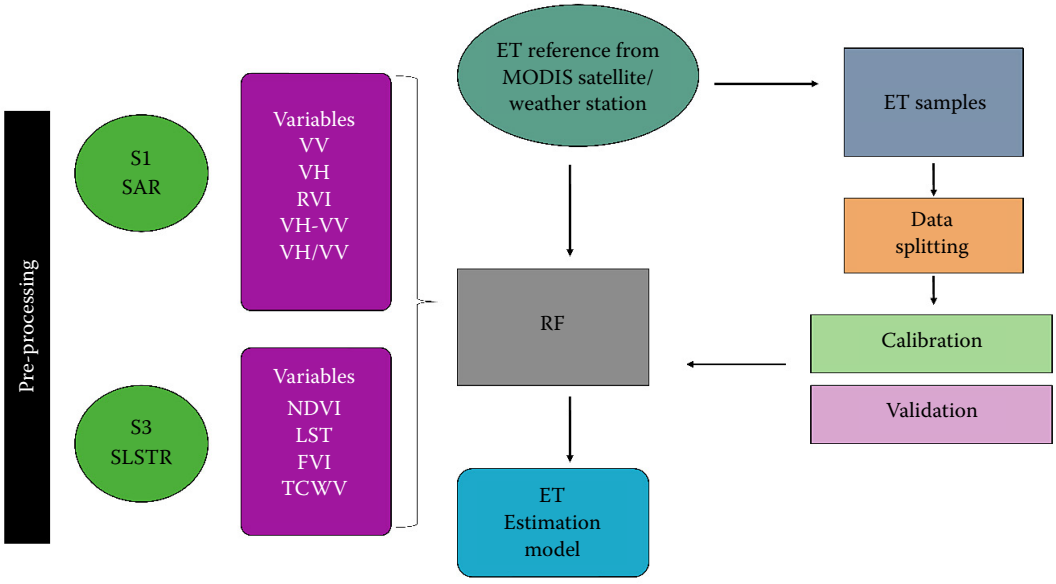


Figure 2. Methodology flow chart of the study

SAR – synthetic aperture radar; SLSTR– sea and land surface temperature radiometer; RF – random forest; ET – evapotranspiration; for remotely sensed variables abbreviations see Table 1

https://doi.org/10.17221/120/2026-RAE

factor. The reference map used geolocations of the geotagged trees from the study area, comprising 70 sample points (Figure 2). Subsequently, the relevant values from remotely sensed variables were extracted. Using the ArcMap software, the database was prepared and exported to MS Visual Studio for the calibration and validation of RF model (Hao et al. 2022). The data collected during the primary sampling (January 2024 to December 2025) were fully utilised to calibrate the model, and for an independent model evaluation, an additional temporally disjoint dataset was prepared three months before (October to December 2023) and after (January to March 2026) the primary sampling period was used for validation. These observations were exclusively used for model validation, providing a more rigorous test of the model's generalisation than the internal random split.

The field-measured ET data were collected from the weather station available at the farm. The data were collected using the Vantage Pro2 Plus Davis weather station (Davis Instruments Corporation, Hayward, CA, USA; https://www.davisinstruments.com). The weather station records variables including precipitation, humidity, wind speed and direction, temperature, and solar insolation. Using all these measured parameters, the weather station calculates the ET using the Penman-Monteith equation (Allen et al. 2001). The field ET data were collected during the same period as the satellite ET. These data were cleaned, with missing values and outliers removed. These data were also split at an 80–20 ratio for model calibration and validation. The equivalent independent evaluation could not be extended to the field-based model because the on-farm weather station was operated only during the primary sampling period, and no field-measured ET records exist for the pre- and post-sampling windows.

Random forest. The random forest (RF) is an ensemble learning technique that utilises multiple decision trees and aggregates their prediction results. Every tree of the forest is built by a technique called bootstrap aggregating (bagging), where a random sample with replacement, Di, of the training data D is selected, and $|Di| = |D|$. Instead of considering all features to partition the data, a random sample of features, $m = \sqrt{p}$ (where p is the number of features), is used on each node in a tree, and this further randomisation is implemented.

At each node where the split is determined, there is typically a criterion that uses either Gini impurity (classification) or mean squared error (MSE) (regression). Gini impurity to classify is calculated as

$$E = -\sum_{i=1}^{c} p_i \times \log(p_i) \quad (1)$$

where: c – the number of distinct classes; p_i – the prior probability for each class.

In regression, the splitting criterion is used to minimise the MSE, which is calculated as

$$\text{MSE} = \left(\frac{1}{c}\right)\sum_{i=1}^{c}(y_i - \bar{y})^2 \quad (2)$$

where: y_i – the actual values; $\bar{y}$ – the mean prediction.

Any tree reaches its optimum depth without being trimmed. Majority voting is the last classification prediction.

$$\bar{y} = \text{mode}(h_1(x), h_2(x), ..., h_k(x)) \quad (3)$$

where: $h_i(x)$ – the prediction made by the i^{th} tree.

The last prediction is obtained as the average of the predicted values in the regression.

$$\bar{y} = (1/k)\ h_i(x) \quad (4)$$

The error rate of the RF algorithm is determined by the interaction between trees(r) and the strength of a single tree (s). The error due to generalisation is restricted by the formula:

$$\rho(1 - s^2)/s^2 \quad (5)$$

RF offers a measure of feature importance by the mean decrease impurity (MDI), which is defined as:

$$\text{MDI}_j = \sum\left(\frac{n_t}{N}\right) \times \Delta i_t \text{ for feature } j \quad (6)$$

where: n_t – the number of samples at node t; N – the total sample count; Δi_t – the impurity reduction at node t.

Out of bag (OOB) error estimates rely on samples excluded from each tree's bootstrap sample,

https://doi.org/10.17221/120/2026-RAE

Table 2. Descriptive statistics of evapotranspiration data

Mean	Median	Standard deviation	Minimum	Maximum	Skewness
3.944	4.012	0.697	2.488	5.800	–0.131

offering an unbiased assessment of generalisation error without requiring a separate validation set.

RESULTS AND DISCUSSION

Descriptive statistics. The ET data exhibited a near-normal distribution with slight negative skewness (–0.131), a mean of 3.944 mm, and values ranging from 2.488 to 5.800 mm (Table 2, Figure 3), indicating meaningful spatial variability across the study area suitable for RF model training. The remotely sensed predictor variables spanned equally wide ranges, NDVI varied from 0.11 to 0.72, reflecting contrasting vegetation densities, LST ranged from 15.3 to 33.7 °C, capturing the thermal variability that drives evaporative demand, and SAR backscatter coefficients (VV –12.6 to 0.36 dB, VH –20.74 to 0.13 dB) alongside derived indices (RVI 0.30 to 3.55, VH-VV –12.7 to 5.26) represented diverse vegetation structure and moisture conditions. Together, this combination of optical, thermal, and radar variables provides a comprehensive characterisation of the biophysical and environmental factors governing ET, forming a robust input dataset for the RF modelling framework.

Model training using a random search. Hyperparameter optimisation was performed using a random grid search, which was preferred over conventional grid search for its ability to efficiently explore the configuration space at lower computational cost (Wang et al. 2025). Key RF parameters such as the number of trees, maximum depth, minimum samples split, minimum samples per leaf, maximum features, and bootstrap were tuned to balance model performance and prevent overfitting (Alavi et al. 2024). The optimised configuration yielded 1 183 trees, unlimited maximum depth, a minimum sample split of 6, a minimum leaf sample of 1, square-root maximum features, and no bootstrapping.

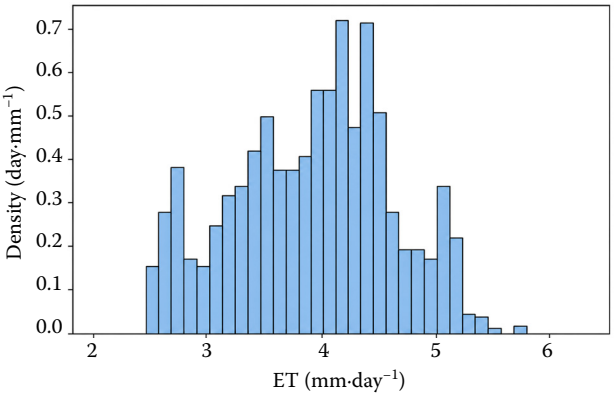


Figure 3. Distribution of evapotranspiration (ET) data

Influence of variables on the model. The RF model of ET estimation was calibrated using the weather station in the study area; the resulting statistical values of the model were highly significant. To predict and view the effect of the explanatory variable on the ET estimation model, a split criterion was used. Figure 4 shows the effect of variables on the ET estimation model, from the most significant to the least significant. The larger the value, the greater the power of the response and explanatory variable. As shown in Figure 4, NDVI is the most significant explanatory variable and the most important for modelling and estimating ET. This variable aligns with the dry and wet seasons in the area, as when it is low, it indicates a depletion of precipitation. The variables LST and TCWV also had a significant impact on the ET model, as their variations directly affect ET values (Rafalia et al. 2025). This shows the great

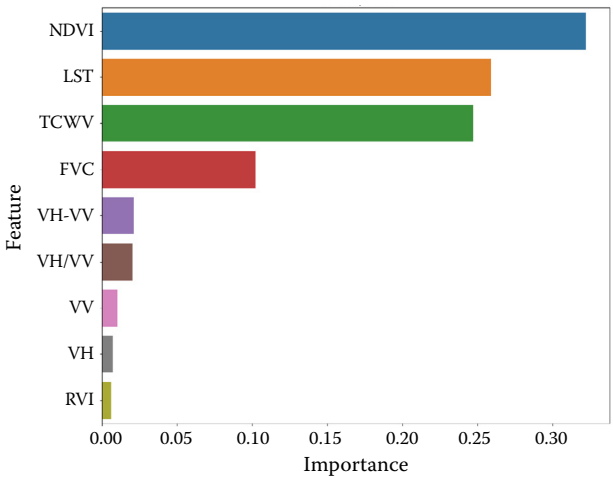


Figure 4. Degree of importance of remotely sensed variables based on the random forest (RF) model

For remotely sensed variables abbreviations see Table 1

https://doi.org/10.17221/120/2026-RAE

potential of these variables and this model in different applications of agronomy (Douna et al. 2021).

In cold, low soil water availability areas with inadequate precipitation, the LST enhances ET. The difference in LST is quite reliant on vegetative transpiration and the surface energy exchange between incoming and outgoing energy (Pande et al. 2024). High radiation under drought conditions causes excessive surface drying, thus causing a higher ET rate and lower soil moisture, consequently leading to an increase in temperature and heat flux (Bellvert et al. 2025). According to research by (Chintala et al. 2022) NDVI and SAR backscatter could be used to detect various physical environmental conditions, because they are both related to optical plant properties. The study by (Zhao et al. 2022) indicated that the difference in the values of NDVI plays a major role in determining the spatial variability of the ET rates. The randomness of the scattering is measured by the RVI, which was the least affected variable, then the VV and VH polarisations, which are considered in relation to vegetation conditions. The relationship of RVI with other indices is determined by the fact that the indices should be independent of soil moisture and surface roughness (Shamsaie and Ghaderi 2025). The VH polarisation can have a low impact on the ET on sloppy terrain and rough surfaces (highly reflective surfaces) since the polarisation is strongly reflected and there is multiple scattering. This is consistent with the saturation behaviour reported by (Chintala et al. 2022), because the dense durian canopy presents a relatively smooth, highly reflective surface to the radar signal; VH backscatter and the RVI derived from it are prone to multiple scattering and signal saturation, which would reduce their sensitivity to canopy variation and help explain why they contributed comparatively little predictive power relative to the optical indices in the RF model.

Figure 5 shows the correlation between ET and remotely sensed variables. ET had a positive relationship with NDVI and LST. A study by (Anees et al. 2024) based on MODIS imagery revealed that NDVI has a positive correlation with ET. It was also reported that the LST is a force impacting ET, which positively

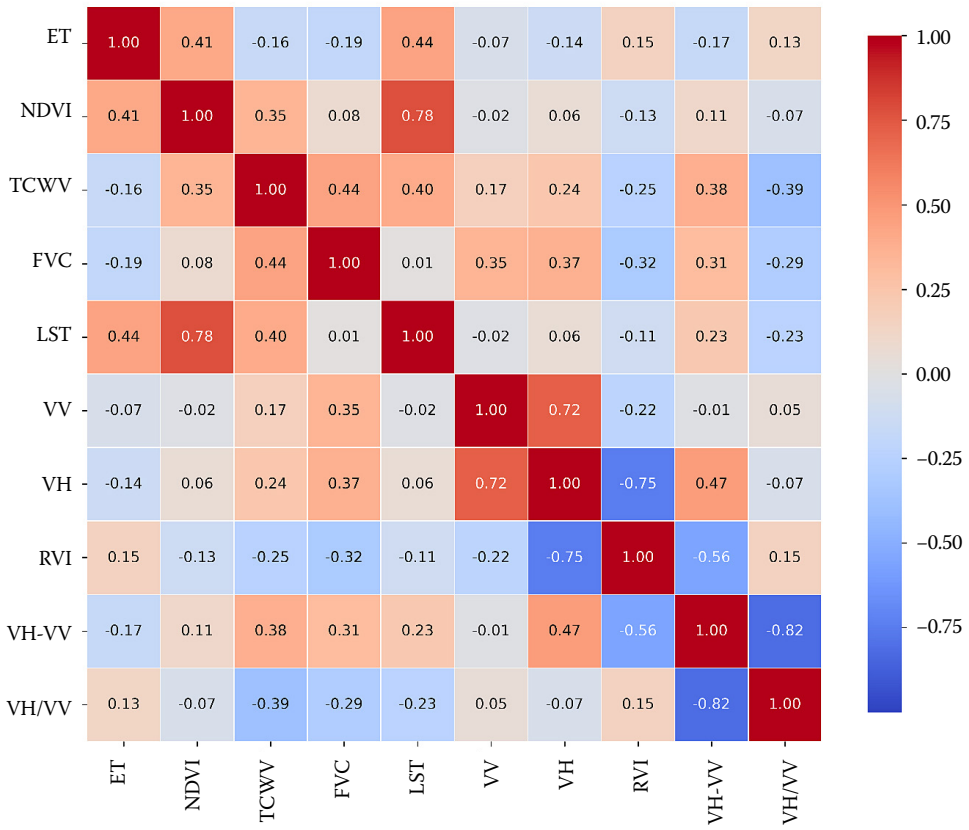


Figure 5. Correlation between evapotranspiration and remotely sensed variables
For remotely sensed variables abbreviations see Table 1

https://doi.org/10.17221/120/2026-RAE

impacts variation (Allam et al. 2021). Jaafar et al. (2022) identified that in water scarce areas the LST had a negative correlation to ET. Malaysia receives approximately 3 000 mm of rainfall annually (Abdul Karim and Tamin 2024), and this is the reason why there was a positive relationship between ET and LST. However, the relationship of ET with RVI, VH, VH-VV, VH/VV, FVC, and TCWV was weak.

Model accuracy assessment. The spatial distribution of ET can be estimated using the RF model. This is envisioned to contribute to the wise use of water systems. Model performance in this study was evaluated using root mean squared error (RMSE) and correlation coefficient (r). Two RF models were constructed and tested to predict ET; one of these was calibrated with the input of satellite reference data derived by MODIS and the other with the input of the field-measured ET data. The satellite-based RF model created a significant correlation between Sentinel-1 and Sentinel-3 satellite measurements and the reference data on the source of ET from MODIS. The calibration dataset comprising all the data during the primary sampling achieved an RMSE of 0.191 mm and an r value of 0.971, indicating the model reproduced Sentinel-based ET values with high precision. The relationship between MODIS ET and Sentinel-derived ET in calibration is depicted in Figure 6A. To evaluate the model's ability to generalise beyond the calibration period, the model was subsequently tested on the temporally independent dataset from three months before and three months after the primary sampling period. On this fully unseen dataset, the model achieved an RMSE of 0.885 mm and an r of 0.913 (Figure 6B). The independent validation error is slightly higher than the calibration error, and Figure 6B shows a somewhat wider scatter around the 1 : 1 line than the calibration plot (Figure 6A), particularly among the lower ET values near 2 mm, where several points fall below the line. This is attributable to seasonal differences between the training and independent evaluation windows. Despite this increase in scatter, an r value of 0.913 on genuinely unseen, out-of-season data still indicates a reasonably strong and practically useful degree of temporal transferability. This issue can be overcome with the development of sensors and advanced AI constructs, which will create an opportunity to conduct additional research in the field of agroclimatic modelling (Nozari et al. 2022). Overall, the strong calibration statistics together with a genuinely independent, out-of-season validation illustrate both the accuracy and the reasonable temporal transferability of the adopted methodology, supporting its use as a guide for other research undertakings that aim to model and map ET distribution under comparable climatic and environmental conditions.

To further strengthen the robustness and credibility of the proposed modelling framework, a second RF model was developed using field-measured ET data as the reference, replacing the MODIS-derived values used in the primary model. This approach provides ground truth validation and enables a direct evaluation of the model's

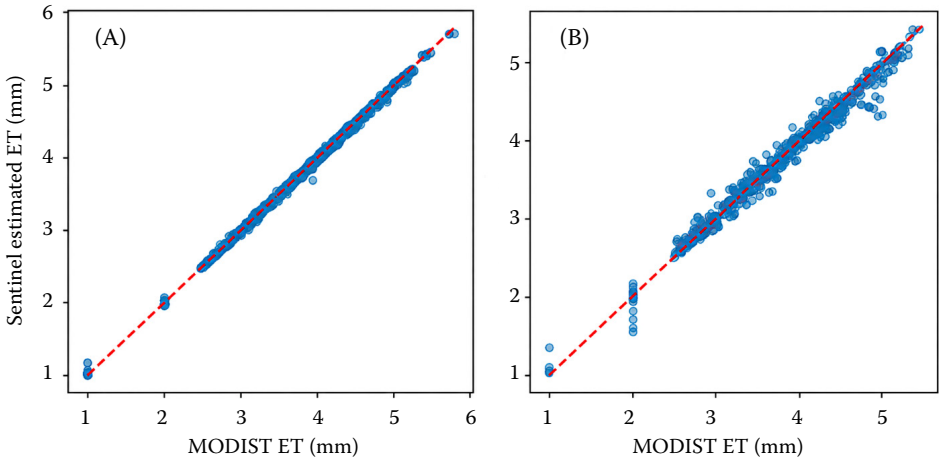


Figure 6. Relationship between MODIS ET and Sentinel estimated evapotranspiration (ET) values for (A) model calibration and (B) model validation using a temporally independent dataset

https://doi.org/10.17221/120/2026-RAE

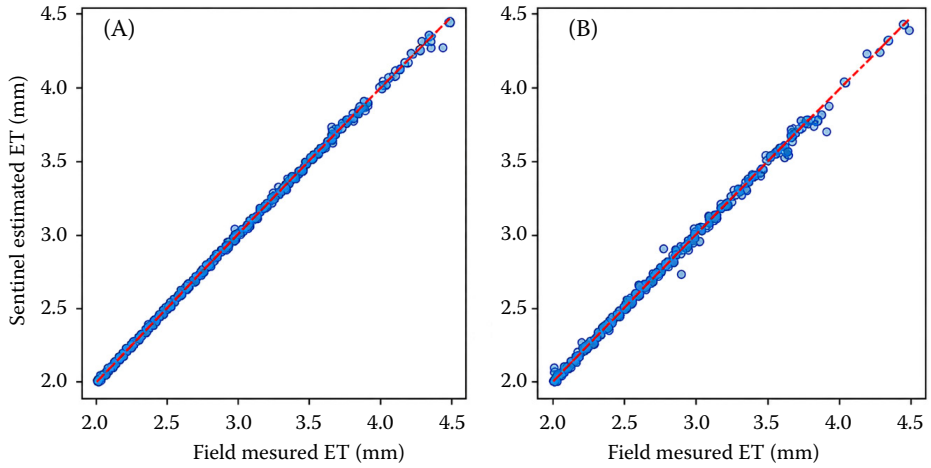


Figure 7. Relationship between field-measured evapotranspiration (ET) and Sentinel-estimated ET values for (A) model calibration (80% of dataset) and (B) model validation (20% of dataset)

ability to predict outcomes against actual in-situ observations. The field-based RF model demonstrated exceptional performance during calibration, achieving an *r* value of 0.990 and an RMSE of 0.710 mm (Figure 7A). These results indicate that the model was highly capable of capturing the variance inherent in the field-measured ET data, with an almost exact match between input and output values. The extremely low RMSE further confirms that the model's predictions are highly consistent with ground level measurements and minimal systematic error. During validation, the field-based model achieved an r value of 0.998 and RMSE of 0.215 mm, with the validation *r* value marginally exceeding that of calibration (0.990), indicating strong generalisation without overfitting (Figure 7B). The close agreement between the satellite-based and field-based model results confirms the reliability and transferability of the RF framework for ET estimation in tropical durian orchards and similar environments.

CONCLUSION

The study focused on estimating ET from Sentinel-1 GRD and Sentinel-3 SLSTR Level 2 data within a durian orchard in Malaysia. In line with the first objective, Sentinel-1 SAR and Sentinel-3 SLSTR data were successfully integrated with an RF algorithm to estimate ET in the orchard, and, addressing the second objective, the performance of the RF model calibrated with satellite-derived ET data was directly compared against the model calibrated with field-measured ET data. Two RF models were constructed and assessed, a primary one based on satellite data, and another on field data. Strong correlations were recorded between the actual ET and the models estimated ET in all the calibration and validation datasets for both models. The satellite model recorded calibration and validation r values of 0.971 and 0.913 with RMSE values of 0.191 mm and 0.885 mm, respectively. The validation was performed using a temporally independent dataset drawn from three months before and after the primary sampling period rather than from a random internal split, providing a stringent test of the model's ability to generalise across seasons and time. The field-based model displayed an *r* value of 0.990 in calibration and 0.998 in validation, and RMSE values of 0.710 mm and 0.215 mm, respectively, using the same internal data splitting, since the on-farm weather station was operated only during the primary sampling period and could not supply independent pre- or post-sampling records. The similar accuracy of both models highlighted the robustness of the RF framework, reaffirming its capacity to reliably capture ET at the satellite and local field levels. This study shows that VV polarisation is the least important in estimating ET while NDVI is the most important. To achieve optimised accuracy in estimating ET, more studies using various deep learning and machine learning models are necessary. The integration of multi-sensor data with varying spatial and radiometric resolutions may introduce preprocessing errors,

https://doi.org/10.17221/120/2026-RAE

potentially reducing model accuracy. As a predictive ML model, the RF framework is limited in its ability to fully generalise the relationship between ET and SAR/SLSTR spectral data, which could be addressed in future studies by expanding the training database and refining hyperparameter optimisation procedures. Optimised water management is possible with an accurate ET estimation methodology. This study also provides better knowledge of ET assessment using the Sentinel-1 and Sentinel-3 satellites in irrigation management. Accurate ET estimation is critical in establishing irrigation scheduling, water use efficiency, and water productivity.

Acknowledgement

The authors would like to thank the Editors, Assistant Editors, and anonymous reviewers for their support and constructive comments that helped improve the quality of this scientific article.

REFERENCES

Abdul Karim S.A., Tamin O. (2024): Malaysia's rainfall and Kalumpang agricultural station data for scattered data interpolation. Data in Brief, 56: 110840.

Aguirre-García S.D., Aranda-Barranco S., Nieto H., Serrano-Ortiz P., Sánchez-Cañete E.P., Guerrero-Rascado J.L. (2021): Modelling actual evapotranspiration using a two source energy balance model with Sentinel imagery in herbaceous-free and herbaceous-cover Mediterranean olive orchards. Agricultural and Forest Meteorology, 311: 108692.

Alavi M., Albaji M., Golabi M., Ali Naseri A., Homayouni S. (2024): Estimation of sugarcane evapotranspiration from remote sensing and limited meteorological variables using machine learning models. Journal of Hydrology, 629: 130605.

Allam M., Mhawej M., Meng Q., Faour G., Abunnasr Y., Fadel A., Xinli H. (2021): Monthly 10-m evapotranspiration rates retrieved by SEBALI with Sentinel-2 and MODIS LST data. Agricultural Water Management, 243: 106432.

Allen R.G., Smith M., Pereira L.S., Raes D., Wright J.L. (2001): Revised FAO Procedures for Calculating Evapotranspiration: Irrigation and Drainage Paper No. 56 with Testing in Idaho. In: Proceedings Watershed Management and Operations Management 2000: 1–10.

Anees S.A., Mehmood K., Rehman A., Rehman N.U., Muhammad S., Shahzad F., Hussain K., Luo M., Alarfaj A.A., Alharbi S.A., Khan W.R. (2024): Unveiling fractional vegetation cover dynamics: A spatiotemporal analysis using MODIS NDVI and machine learning. Environmental and Sustainability Indicators, 24: 100485.

Bai Y., Mallick K., Hu T., Zhang S., Yang S., Ahmadi A. (2024): Integrating machine learning with thermal-driven analytical energy balance model improved terrestrial evapotranspiration estimation through enhanced surface conductance. Remote Sensing of Environment, 311: 114308.

Bellvert J., Pamies-Sans M., Casadesús J., Girona J. (2025): Evaluating the impact of drought and water restrictions on agricultural production in irrigated areas through crop water productivity functions and a remote sensing-based evapotranspiration model. Agricultural Water Management, 309: 109319.

Bu J., Gan G., Chen J., Su Y., Yuan M., Gao Y., Domingo F., López-Ballesteros A., Migliavacca M., El-Madany T.S., Gentine P., Xiao J., Garcia M. (2024): Dryland evapotranspiration from remote sensing solar-induced chlorophyll fluorescence: Constraining an optimal stomatal model within a two-source energy balance model. Remote Sensing of Environment, 303: 113999.

Chintala S., Harmya T.S., Kambhammettu B.V.N.P., Moharana S., Duvvuri S. (2022): Modelling high-resolution evapotranspiration in fragmented croplands from the constellation of Sentinels. Remote Sensing Applications: Society and Environment, 26: 100704.

Chipula G., Moyo V., Reuben T.N., Fiwa L., Nkhata M., Phiri H., Fandika I. (2025): Development and evaluation of site-specific evapotranspiration models in Malawi through a comparative analysis of existing models. Physics and Chemistry of the Earth, Parts A/B/C, 137: 103814.

Das S., Kaur Baweja S., Raheja A., Gill K.K., Sharda R. (2023): Development of machine learning-based reference evapotranspiration model for the semi-arid region of Punjab, India. Journal of Agriculture and Food Research, 13: 100640.

dos Santos E.P., Moreira M.C., Fernandes-Filho E.I., Demattê J.A.M., Santos U.J. dos, Moura-Bueno J.M., Cruz R.R.P., Silva D.D. da, Sampaio E.V. de S.B. (2025): Integrating satellite radar vegetation indices and environmental descriptors with visible-infrared soil spectroscopy improved organic carbon prediction in soils of semi-arid Brazil. Geoderma, 457: 117288.

Douna V., Barraza V., Grings F., Huete A., Restrepo-Coupe N., Beringer J. (2021): Towards a remote sensing data based evapotranspiration estimation in Northern Australia using a simple random forest approach. Journal of Arid Environments, 191: 104513.

Fan D., Zhao T., Jiang X., García-García A., Schmidt T., Samaniego L., Attinger S., Wu H., Jiang Y., Shi J., Fan L., Tang B. H., Wagner W., Dorigo W., Gruber A., Mattia F.,

https://doi.org/10.17221/120/2026-RAE

Balenzano A., Brocca L., Jagdhuber T., Wignerton J., Montzka C., Peng J. (2025): A Sentinel-1 SAR-based global 1-km resolution soil moisture data product: Algorithm and preliminary assessment. Remote Sensing of Environment, 318: 114579.

Fuentes S., Ortega-Farías S., Carrasco-Benavides M., Tongson E., Gonzalez Viejo C. (2024): Actual evapotranspiration and energy balance estimation from vineyards using micro-meteorological data and machine learning modeling. Agricultural Water Management, 297: 108834.

Guo J., Fan L., Feng P., Sun X., Xue S. (2025): Response of vegetation evapotranspiration to landscape pattern changes in an arid region: A case study of the Loess Plateau, China. Catena, 252: 108878.

Guo N., Chen H., Han Q., Wang T. (2024): Evaluating data-driven and hybrid modeling of terrestrial actual evapotranspiration based on an automatic machine learning approach. Journal of Hydrology, 628: 130594.

Guzinski R., Nieto H. (2019): Evaluating the feasibility of using Sentinel-2 and Sentinel-3 satellites for high-resolution evapotranspiration estimations. Remote Sensing of Environment, 221: 157–172.

Hailegnaw N.S., Bayabil H.K., Berihun M.L., Teshome F.T., Shelia V., Getachew F. (2024): Integrating machine learning and empirical evapotranspiration modeling with DSSAT: Implications for agricultural water management. Science of The Total Environment, 912: 169403.

Hao P., Di L., Guo L. (2022): Estimation of crop evapotranspiration from MODIS data by combining random forest and trapezoidal models. Agricultural Water Management, 259: 107249.

Hu X., Ren H., Tansey K., Zheng Y., Ghent D., Liu X., Yan L. (2019): Agricultural drought monitoring using European Space Agency Sentinel 3A land surface temperature and normalized difference vegetation index imageries. Agricultural and Forest Meteorology, 279: 107707.

Jaafar H., Mourad R., Schull M. (2022): A global 30-m ET model (HSEB) using harmonized Landsat and Sentinel-2, MODIS and VIIRS: Comparison to ECOSTRESS ET and LST. Remote Sensing of Environment, 274: 112995.

Jia Y., Su Y., Zhang R., Zhang Z., Lu Y., Shi D., Xu C., Huang D. (2022): Optimization of an extreme learning machine model with the sparrow search algorithm to estimate spring maize evapotranspiration with film mulching in the semiarid regions of China. Computers and Electronics in Agriculture, 201: 107298.

Kebede N., Ayana M., Mekonnen B. (2025): Quantification of onion (*Allium cepa* L.) evapotranspiration and crop coefficient via weighable lysimeter under semi-arid climate of Melkasa, Ethiopia. Heliyon, 11: e42566.

Knipper K., Anderson M., Bambach N., Melton F., Ellis Z., Yang Y., Volk J., McElrone A.J., Kustas W., Roby M., Carrara W., Castro S., Kilic A., Fisher J.B., Ruhoff A., Senay G.B., Morton C., Saa S., Allen R.G. (2024): A comparative analysis of OpenET for evaluating evapotranspiration in California almond orchards. Agricultural and Forest Meteorology, 355: 110146.

Musyimi P.K., Sahbeni G., Timár G., Weidinger T., Székely B. (2022): Actual Evapotranspiration estimation using Sentinel-1 SAR and Sentinel-3 SLSTR data combined with a gradient boosting machine model in Busia County, Western Kenya. Atmosphere, 13: 1927.

Naghdyzadegan Jahromi M., Zand-Parsa S., Razzaghi F., Jamshidi S., Didari S., Doosthosseini A., Pourghasemi H.R. (2023): Developing machine learning models for wheat yield prediction using ground-based data, satellite-based actual evapotranspiration and vegetation indices. European Journal of Agronomy, 146: 126820.

Nozari S., Bailey R.T., Haacker E.M.K., Zambreski Z.T., Xiang Z., Lin X. (2022): Employing machine learning to quantify long-term climatological and regulatory impacts on groundwater availability in intensively irrigated regions. Journal of Hydrology, 614: 128511.

Pande C.B., Egbueri J.C., Costache R., Sidek L.M., Wang Q., Alshehri F., Din N.M., Gautam V.K., Chandra Pal S. (2024): Predictive modeling of land surface temperature (LST) based on Landsat-8 satellite data and machine learning models for sustainable development. Journal of Cleaner Production, 444: 141035.

Rafalia N., Moumen I., Chatoui Y., Abouchabaka J. (2025): Enhancing precision in evapotranspiration estimation: AI-powered downscaling of VIIRS LST. Scientific African, 27: e02590.

Rahman M., Hasan M.M., Hossain M.A., Das U.K., Islam M.M., Karim M.R., Faiz H., Hammad Z., Sadiq S., Alam M. (2025): Integrating deep learning algorithms for forecasting evapotranspiration and assessing crop water stress in agricultural water management. Journal of Environmental Management, 375: 124363.

Shamsaie R., Ghaderi D. (2025): Comparison of efficiency of spectral (NDWI) and SAR (GRD) method in shoreline detection: A novel method of integrating GRD and SLC products of Sentinel-1 satellite. Regional Studies in Marine Science, 84: 104132.

Shang S., Zhu G., Zhang K., Chen H., Wang Y., Chen Y., Zhang Z., Ma N. (2024): Spatial-temporal variations in evapotranspiration across the continental United States: An atmospheric water balance perspective. Journal of Hydrology, 640: 131699.

Silva T.G.F. da, Queiroz M.G. de, Zolnier S., Jardim A.M. da R.F., Santos W.R. dos, Moura M.S.B. de, Souza C.A.A. de,

https://doi.org/10.17221/120/2026-RAE

Steidle Neto A.J., Araújo Júnior G. do N., Silva M.J. da, Salvador K.R. da S., Silva E.F. da, Souza L.S.B. de (2025): Energy balance and evapotranspiration conditioned by deforestation of a seasonally dry tropical forest (Caatinga): A series of four water seasons. Journal of South American Earth Sciences, 157: 105474.

Wang Y., Zou B., Xu J., Xu C., Tang Y.Y. (2025): ALR-HT: A fast and efficient Lasso regression without hyperparameter tuning. Neural Networks, 181: 106885.

Woldemariam G.W., Awoke B.G., Maretto R.V. (2025): Satellite-based energy balance for estimating actual sugarcane evapotranspiration in the Ethiopian Rift Valley. ISPRS Journal of Photogrammetry and Remote Sensing, 223: 109–130.

Zhao T., Zhu Y., Ye M., Yang J., Jia B., Mao W., Wu J. (2022): A new approach for estimating spatial-temporal phreatic evapotranspiration at a regional scale using NDVI and water table depth measurements. Agricultural Water Management, 264: 107500.

Zolfaghari A.A., Raeesi M., Longo-Minnolo G., Consoli S., Dyck M. (2025): Daily reference evapotranspiration prediction in Iran: A machine learning approach with ERA5-land data. Journal of Hydrology: Regional Studies, 59: 102343.

Received: May 8, 2026
Accepted: August 26, 2026
Published online: November 18, 2026